LAMS-2619

C.3

LOS ALAMOS SCIENTIFIC LABORATORY

OF THE UNIVERSITY OF CALIFORNIA o LOS ALAMOS NEW MEXICO

QUARTERLY STATUS REPORT OF THE LASL CONTROLLED THERMONUCLEAR RESEARCH PROGRAM FOR PERIOD ENDING AUGUST 20, 1961

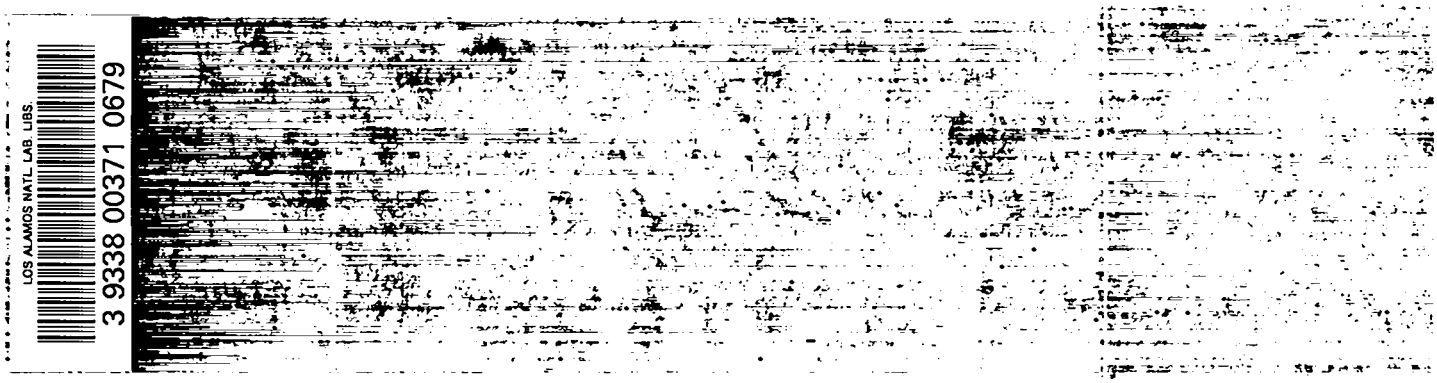

Printed in USA. Price $ 1.00. Available from the

Office of Technical Services
U. S. Department of Commerce
Washington 25, D. C.

LAMS-2619
CONTROLLED THERMONUCLEAR
PROCESSES
(TID-4500, 16th Ed.)

LOS ALAMOS SCIENTIFIC LABORATORY
OF THE UNIVERSITY OF CALIFORNIA LOS ALAMOS NEW MEXICO

REPORT COMPILED: September 1961
REPORT DISTRIBUTED: September 29, 1961

QUARTERLY STATUS REPORT OF THE LASL CONTROLLED THERMONUCLEAR RESEARCH PROGRAM FOR PERIOD ENDING AUGUST 20, 1961

Prepared from material submitted by members of P Division

Contract W-7405-ENG. 36 with the U. S. Atomic Energy Commission

SHERWOOD PROGRAM QUARTERLY REPORT

SUMMARY

1. Stability studies have been made of the plasma jet from a hydromagnetic gun as it passes through either converging or diverging axial magnetic fields in the caulked picket fence system. Results show that the plasma boundary is more stable in the converging field but there is focusing or guiding of the jet by both types of fields. Photographs of the jet colliding with a target after passing through either the converging or diverging fields strongly suggest that flute instabilities occur in both cases.

2. Time-resolved measurements of Doppler broadening of the He II 4686 A line in the full-scale model caulked picket fence show confinement times of $\geq$ 40 μsec for He ions of ~ 330 ev energy. The average ion energy then drops rapidly with a characteristic time of ~ 50 μsec due to the influx of cold He ions and impurities.

3. In the Mark II (bakeable) picket fence experiment, confinement times of deuterium plasma injected into the system from hydromagnetic guns have been determined from measurements of the neutrons produced by D-D reactions. For one gun injection, the time behavior of the neutron yield indicates confinement with a typical decay period of ~ 40 μsec corresponding to about 80 reflections within the picket fence confining field system. With two-gun injection -- at the two point cusps of the machine -- the prompt collision pulse of neutrons dominates the yield obtained but a delayed neutron yield is observed with a time constant of ~ 20 μsec.

4. Experimental work on the orthogonal pinch system using 3-μsec rise time has been terminated. Asymmetries in the coil cross section in the vicinity of the feedpoint are observed to have a strong effect on the neutron yield. The relatively long duration of the neutron emission indicates the existence of a quasi-thermal plasma. The heating is consistent with that expected from an abnormal interdiffusion of fields through the plasma boundary. It is postulated that the angular asymmetry in the B_z field may contribute to the rapid interdiffusion of magnetic fields through the conducting boundary. Work on high-current, low-inductance spark gaps of higher operating voltages -- up to 57 kv with pulse charging -- has been carried out.

5. Simultaneous measurements have been made of the incoherently scattered S-band microwaves and incident and reflected 28 Mc/sec rf power in the scattering chamber. A scattering resonance has been observed associated with a strong impedance mismatch brought about by a sudden change in the impedance of the discharge when rf electric fields become large in the plasma. Further work is underway to search for plasma oscillation effects in the incoherently scattered spectrum, and for strong resonances in plasma dielectric constant for arbitrary angles between propagation vector and magnetic field.

6. Statistical mechanics analysis based on Liouville's theorem, similar to that used in accelerator design, has been applied to the resonant helix injection device to determine the maximum particle densities that can be obtained in such a system with practical ion sources. Results indicate maximum theoretical densities of $\sim 10^{11}$ particles/cm^3. Loss mechanisms not included in the theory would make the realizable densities significantly less than this. The indicated dependence of the density obtained on the acceptance area of the injector determined by the mirror ratio is being investigated experimentally.

7. Probe measurements and time resolved photographs of the plasma in motion down the barrel of the coaxial hydromagnetic gun indicate an unstable spoke discharge rather than a uniform plasma region with initial gas densities $\leq 10^{14}$ particles/cm^3. Measurements of plasma jet penetration through a transverse magnetic field show that the jet penetrates through a 500-gauss barrier without measurable loss in density but is either stopped or deflected outside the acceptance area of the detector by a 1000-gauss barrier. With a transverse field of intermediate magnitude (750 gauss), the plasma jet penetrates through without loss in intensity but is delayed in time.

8. The electron temperature (T_e) of Scylla III has been measured with the beryl crystal x-ray spectrometer and by a two-absorber soft x-ray detector. The values (about 500 ev) were somewhat higher than those in Scylla I. Measurements as a function of time showed an abrupt drop in T_e when instabilities set in. In those cases where the plasma was moderately stable, T_e follows a sinusoidal decompression from peak field.

9. The two-gun plasma collision apparatus has been adapted to the injection of plasma into Scylla III. Both fast and slow components in the plasma have been trapped and compressed in the magnetic field with the production of neutrons.

10. Operation of the E x B apparatus has been markedly improved by withdrawing the coaxial gun injector from the region of transverse E and B fields, thus eliminating shorting of the transverse E field by the gun electrode. Plasma is now transmitted through the E x B region and its momentum is increased a factor of 3 to 4 over the momentum of plasma from the coaxial gun without crossed E and B fields.

11. An unsuccessful search was made of the visible spectrum from Scylla I in an attempt to find untabulated lines of Ne IX. Such lines would be suitable for measurement in the Zeeman effect experiment.

12. Progress is being made in the design of various components of the 3.5-megajoule Scylla IV magnetic compression experiment.

A. CAULKED PICKET FENCE

Experimental observations have been made on the relative stability of a plasma jet from a hydromagnetic gun injected into converging and diverging axial magnetic fields within the half-scale model caulked picket fence machine. The gun used in the experiments had the same valve and barrel structure used previously but the associated condenser bank was changed to 28 μf with ignitron switching. The diagnostic techniques used in the stability observations were as follows: calorimeter-thermocouple for measurements of energy incident on a target as a function of distance from the gun muzzle, magnetic field probes for study of jet reproducibility in the field configurations, and time-resolved and time-integrated photographs of the luminous region resulting from impact of a He plasma jet on a target inserted in the machine. The plasma boundary is more stable with the converging field than with the diverging field, but some focusing of the central core is maintained in both cases. Probe measurements show that the reproducibility is greater in the converging field. However, distortions observed in the photographs of the plasma jet colliding with the target suggest the existence of flute instabilities with both the converging and diverging fields.

With hydromagnetic gun injection of a He plasma into the full scale model, estimates of the temperature of trapped He ions were obtained from time-resolved measurements of Doppler broadening of the He II 4686 A line. The He ions of 330 ev energy were confined for $\gtrsim 40$ μsec, which is approximately equivalent to at least 7 reflections within the confining field. The average energy of the ions subsequently dropped, with a characteristic time of ~ 50 μsec. Experimental evidence was obtained relating this rapid fall off in temperature to an influx of cold He ions and impurities.

B. BAKEABLE PICKET FENCE

The coaxial plasma guns described in LAMS-2570 (p. 9), with plasma jet outputs containing a high-density component consistent with 10^{13} deuterons/cm^3 at an energy of 25 kev, with neutron yield as a diagnostic tool, are being used for the basic experiments of injection, trapping, and confinement of an energetic plasma in a picket fence confining field, i.e., the "entropy trapping" experiment. Preliminary experiments include the use of either one or two opposing high-speed plasma guns injecting into the picket fence field. The apparatus used is shown in Fig. 1.

Results with One-Gun Operation

1. Average yield ~ 10^6 neutrons/shot with plasma incident on a 3-3/4 in. o.d. Cu calorimeter placed in the center of the picket fence. The main neutron pulse duration is ~ 0.3 μsec. The average energy deposited by the plasma jet is ~ 20 joules. The magnetic field was zero in these experiments.

2. A high-β region is formed by the plasma in the picket fence for cusp fields up to 2 kgauss. The magnetic field perturbation decays with a time constant of ~ 40 μsec.

3. A fast-neutron counter used as a monitor (a 2.5 cm x 5 cm scintillator located at the ring cusp at a radius of 25 cm) indicates a maximum yield of ~ 1.5 x 10^6 neutron/shot with a cusp field of ~ 2 kgauss. The time history of the neutron yield is the major item of interest. On the average the data show a prompt burst (presumably from deuterons striking deuterium on walls), followed in 5-40 μsec by a second rise of neutrons that decay away with mean times (τ) that vary widely from 5-50 μsec, depending on operating conditions. The optimum time duration occurs for fields of ~ 3 kgauss and give ~ 50% of the neutrons in the second pulse which is delayed ~ 15 μsec. This delayed neutron group then decays with $\tau \approx$ 40 μsec. A representative set of data is shown in Fig. 2.

The time history of the neutron yield clearly indicates a trapping of energetic deuterons for many reflections (in the Mark II geometry typically

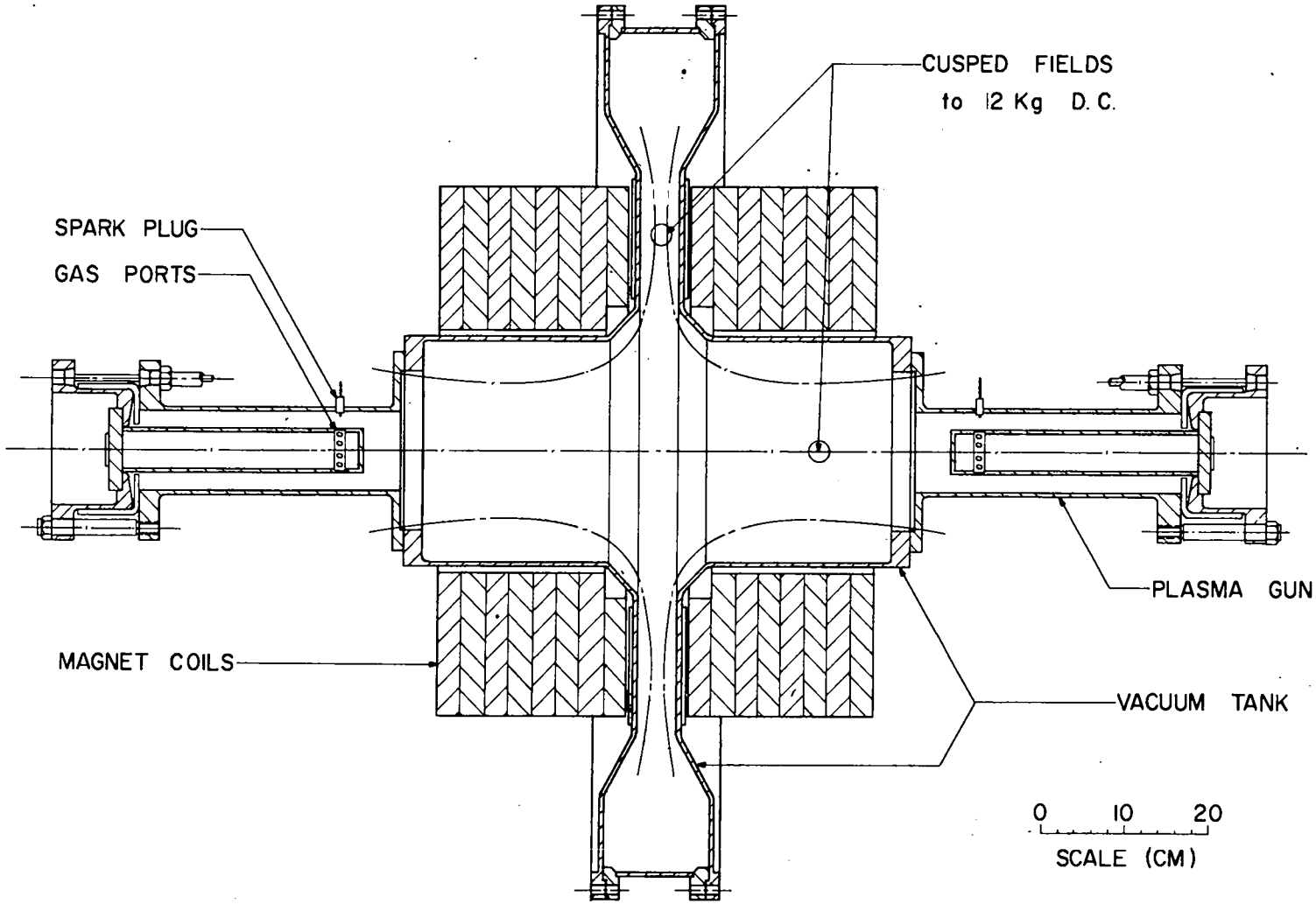

Fig. 1. Apparatus for bakeable picket fence experiment

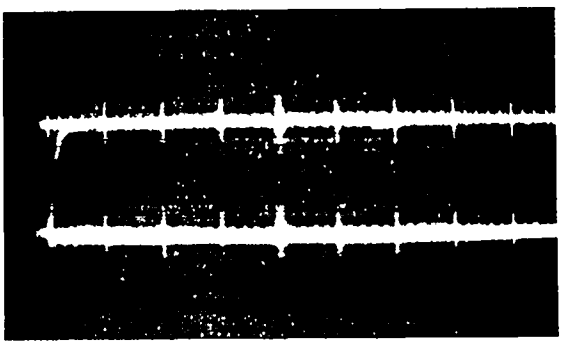

Fast neutron signal

Integrated signal (0.5 volt/cm)
(100 μsec integrator)

Zero magnetic field

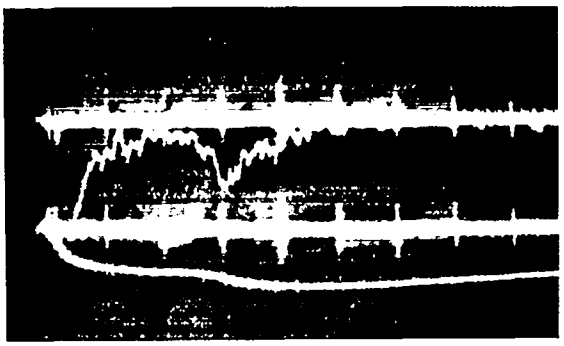

Fast neutron signal

Integrated signal (1.0 volt/cm)
(typical)

2,000 gauss cusp field

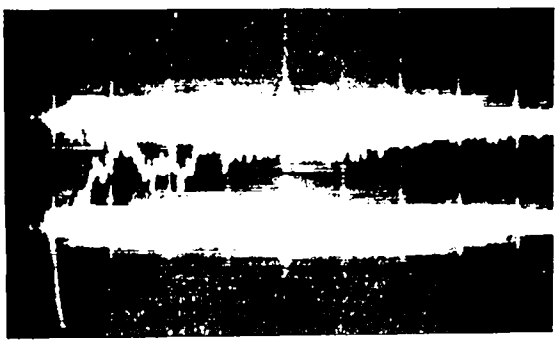

Fast neutron signal

Integrated signal (1 volt/cm)
(off scope)

2,800 gauss cusp field

Sweep speed: 5 μsec/cm

Fast neutron signal smoothed with 0.2 μsec integrator.

Fig. 2. Data obtained with one-gun operation of picket fence experiment

about 80 reflections for $\tau \approx 40$ μsec). However, the analysis of other aspects of the data is subject to a number of difficulties. For example, the prompt burst of neutrons gives rise to a number of delayed capture γ rays from the surrounding materials, which produce a small remnant tail ($\tau \approx 15$ μsec) that must be subtracted from the observed pulse before the neutron yield is determined. Fortunately, the delayed buildup of a second group of neutrons allows an easy separation of this effect, but the occurrence of this second group is not well understood as yet. Also, it has not been determined whether the neutrons are produced in wall or volume interactions; in fact, the fast-neutron counter itself may be acting somewhat as a target which would tend to enhance the effective solid angle. Taking these crude measurements, a preliminary possible fit to the data would be 2×10^{12} deuterons/cm^3 at a kinetic energy of 20 kev in a volume of 10^3 cm^3, assuming volume interactions. More refined experiments are planned to measure these quantities directly.

Results with Two-Gun Operation

The general behavior with two-gun operation was what would be expected from the simple superposition of the two colliding plasma jets acting independently, with two notable exceptions listed below. First, the fast-neutron counter indicated that the maximum neutron yield occurs at about 8.5 kgauss with only a slight decrease up to 10 kgauss. Second, the prompt collision pulse of neutrons in general dominates the neutron yield, although a moderate group of delayed neutrons is observed for fields near 6 kgauss. These neutrons, however, come as a relatively small delayed group decaying with $\tau \approx 20$ μsec and superimposed upon the remnant tail from the initial prompt pulse. Because of the larger substraction involved, little quantitative work has as yet been done with two-gun operation.

C. ORTHOGONAL PINCH EXPERIMENT

The orthogonal pinch experiment which utilized a 3-μsec rise time axial magnetic field (pulsed mirror geometry) has been terminated. Most recent magnetic probe measurements show azimuthal variation of ~ 7-10% in the axial component of the B_z field in the mirror region. Away from the mirror and toward the coil center, the variation becomes negligible. By reducing the thickness of the current feedpoint connection, i.e., by making the physical cross section of the coil and feedpoint connection more axially symmetric, the variation in B_z field with angle is reduced to 1-2%.

The immediate effects of these field perturbations are reflected in the total neutron production. It appears generally that more symmetric coil geometries substantially reduce neutron production. Furthermore, the attachment of radial metal fins along the coil length, which might appear to enhance the field asymmetry due to abrupt changes in coil cross section, has the effect of smoothing the axial magnetic field in azimuth and reducing the total neutron yield. The asymmetry of the coil cross section in the vicinity of the feedpoint plus the size of feedpoint spacing sensitively affects the total neutron yield.

At present, in summary, it is thought that the long duration and slow decay of neutron emission reflects the existence of a quasi-thermal plasma, the density of which is gradually reduced by plasma streaming out the ends (mirror ratio ~ 1). The heating of the plasma is consistent with that obtained through the abnormal interdiffusion of magnetic fields through the plasma boundary while induced θ-currents set up in the residual low-density, highly-conducting plasma near the tube walls may explain the temporary isolation of the plasma during the time B_z is passing through zero and reversing.

It is also felt that the angular asymmetries of the B_z field (mentioned above) in the mirror region may be a new mechanism which can

partially explain the onset of the rapid interdiffusion of magnetic fields through the conducting plasma boundary. It is uncertain whether the azimuthal gradients in the B_z field act hydromagnetically or electromagnetically to bring about the onset of rapid intermixing of plasma and field. By scaling the length of coil, a test of these uncertainties might be affected.

Vacuum Spark Gap

The 20-kv, high-current, low-inductance spark gap of the design used for the past 2-1/2 years has been very successful in switching an energy of 3 kjoules in an array consisting of 10 condensers.

This gap has now been extended to ~ 60 kv using a Sangamo 2-μf, 50 kv condenser. It consists of four electrodes and three glass insulators (cathode, anode, and two floating electrodes). The gap is mounted in high-inductance connection, to limit the condenser current to a reasonable value, and triggered in the usual fashion with a small rail source. With this arrangement, the ringing period is ~ 2.1 μsec which corresponds to a maximum current > 300 kamp at 57 kv. These data were obtained under pulse charging.

The gap has also been operated up to 35 kv dc with no premature breakdown. Operating in a manner similar to the 20-kv gap, the 35-kv gap requires no potential grading of the floating electrodes. A final design of the Sangamo insulator will allow a vacuum gap design of ~ 5 mμh inductance. The Q ($= \pi/\ell_n a_1/a_2$) of the condenser, spark gap, and associated wiring at a frequency of 500 kc is ~ 4, which is rather poor. Whether the resistance is in the gap proper, in the condenser, or both is yet to be determined.

D. COHERENT AND INCOHERENT SCATTERING OF MICROWAVES IN PLASMAS

The 28 Mc/sec rf power incident upon and reflected by the plasma in the scattering chamber and the incoherently scattered microwave signal were measured simultaneously. The sudden onset of the scattering resonance was accompanied by a sudden change in the impedance of the discharge which varied quickly from a good to poor match. This behavior was associated with a sudden change in discharge conditions near the pump-out tube leading to the vacuum system. By installing a metal reflector plate near the mouth of the pump-out tube this discharge condition can be avoided. As a result the onset of the scattering resonance is no longer as sudden, but the resonance remains. It is clear from the rf directional coupler power measurements that the scattering resonance is associated with a strong mismatch, probably of the open circuit kind, and that at this time rf electric fields can drive the plasma profile about its equilibrium value.

To achieve more sensitivity the high power microwave horn has been moved to within 1 ft of the scattering volume. A sensitive matched crystal mixer and IF amplifier with a bandwidth of 2 Mc/sec and a sentivitity of several ^{o}K have also been installed. It is planned to search the incoherently scattered spectrum between the rf excited sidebands for plasma oscillation effects.

Preparations have been continued for an experiment designed to measure the strong resonances (reported from Princeton) in the dielectric constant of a plasma column in a magnetic field for arbitrary angles between propagation vector and magnetic field.

E. RESONANT HELIX EXPERIMENT

Theoretical work on the resonant helix system has been largely concerned with application of statistical mechanics analysis similar to that used in accelerator injection problems.

In any dynamical system of particles whose motions can be described by a Hamiltonian system of equations in the six-dimensional phase space of single particles, Liouville's theorem requires that the density of particles in this phase space be conserved in the neighborhood of each particle trajectory. In connection with the resonant helix experiment, the consequences of this theorem have been explored with regard to the possible existence of a fundamental limit to the maximum achievable density in configuration space for such systems. Consider an ideal magnetic container being supplied by an injection device from an ion source in which the motion of ions is controlled by steady, externally applied electric and magnetic fields. Assume that the specific interactions between pairs of ions, i.e., collisions, can be neglected. Then the system can be described by Hamiltonian equations in six-dimensional phase space. Even the space charge effects which limit the current of ions that can be drawn from the ion source can be represented by a steady self-consistent space charge potential as though it were an externally applied field. Thus the principle of the conservation of density in phase space along each trajectory holds all the way from the ion source into the containment device. It follows then that if a measurable quantity of ions can be injected into the system, then the injection device itself will provide an avenue of escape for the ions, if there are no other leaks in the system.

If the ions are drawn initially from a plasma source in thermal equilibrium at a temperature T_o and density n_o per cm^3, the density distribution in phase space will be given by the Maxwell-Boltzmann law. Suppose that the ions are extracted and accelerated into the magnetic container where the potential energy is $-V$ referred to zero potential energy in the original plasma. Then let the magnetic field re-orient them

until they are isotropic in the available phase space, and assume no losses other than through the injection device. Then the maximum density in configuration space will be

$$n = \int_{\alpha=0}^{2\pi} \int_{\theta=0}^{\pi} \int_{\frac{1}{2}mv^2=V}^{\infty} n_o \left(\frac{m}{2\pi\, k\, T_o}\right)^{3/2} \exp\left[-(1/2\, mv^2 - V)/kT\right] v^2 \sin\theta\, dv\, d\theta\, d\alpha$$

$$= n_o \times 2\pi^{-1/2}\, e^{V/kT}\, \Gamma(3/2, V/kT)$$

$$= n_o \times 2\pi^{-1/2} \left(\frac{V}{kT}\right)^{1/2}, \text{ for large } V.$$

For example, if the ions are drawn from a plasma at 2 ev (to provide nearly 100% ionization) and a density of 10^{13} ions/cm^3 and accelerated to 100 kev, the maximum obtainable density will be

$$n = 10^{13} \cdot \frac{2}{1.77} \left(\frac{10^5}{2}\right)^{1/2}$$

$$= 2.5 \times 10^{15} \text{ ions/cm}^3,$$

about 250 times the density in the original plasma. It would be advantageous to keep the temperature of the plasma source as low as possible consistent with complete ionization.

The conservation of density in phase space argument can be applied specifically to a mirror machine configuration where the mirror ratio determines the acceptance of particles into the region of trapping. The acceptance limitations of the system reduce the maximum achievable densities to a value appreciably less than that obtained above.

Since the phase space density in the injector region of the resonant helix system determines the maximum obtainable density in the magnetic mirror confinement system, the result required can be determined by equating the density equations:

$$\text{Density in injector} = \frac{I(6.2 \times 10^{18})}{(A_i v \Delta\Omega)\,(p^2 \Delta p)},$$

where A_i is the acceptance area of injector, v the approximate average particle speed, $\Delta\Omega$ the acceptance solid angle of injector, p the particle momentum, Δp the momentum spread, and I the current into injector (amp), and

$$\text{Density in magnetic container} = \frac{N}{(A_B \cdot L)(4\pi p^2 \Delta p)} = \frac{n}{4\pi p^2 \Delta p},$$

where A_B is the cross sectional area of available configuration space in mirror system, L the length of system, N the total particles, and n the particle density in configuration space.

It is assumed here that collisions are negligible and that the mirrors and helix distribute the particles randomly in the available phase space indicated. Equating these expressions gives for the maximum configuration space density

$$n = 6 \times 10^{18} \frac{4\pi I}{A_i v \Delta\Omega}.$$

For a high mirror ratio (so that $\Delta\Omega$ is determined by the mirror rather than the helix acceptance), $\Delta\Omega = 2\pi$, the area, A_i, available to a particle in the mirror at the injector end is determined by the Larmor radius of the particle within the mirror field; thus,

$$A_i = \pi\rho^2 = \pi\left(\frac{v}{10^4 H_c R_m}\right)^2,$$

where ρ is the Larmor radius in the central region of the mirror system. Hence,

$$n = 4 \times 10^{26} I \frac{R_m^2 H_c^2}{v^3}.$$

Consider the example

$H = 1000$ gauss $\qquad R_m = 100$

$v = 4.4 \times 10^8$ (100 kev H^+)

Then

$$n = \frac{4(10^6)(10^4)(10^{26})}{100 \times 10^{24}} = 4 \times 10^{10}. \quad \text{per ampere injected}$$

In order to check the dependence of density on mirror ratio indicated by these results, a high mirror ratio (up to ~ 50) experiment is being set up.

F. HYDROMAGNETIC GUN OPERATION

The hydromagnetic gun facility continued to be run under the following conditions:

Capacity	2 μf
Voltage	28 kv
Frequency	570 kc
Induction (total)	3.9×10^{-8} h
Current peak	200 kamp
Pressure, plenum (deuterium)	150-400 mm Hg
Pressure, inter-electrode at firing time	200 μ Hg
Energy, plasma net	5 joules

Four diagnostic techniques were used: calorimeter-thermocouple, magnetic probe, single-particle detector (LAMS-2570), and photography. Data from magnetic probes at positions along the length of the barrel suggested the gun had been operating in an unstable mode; that is, a symmetrical disc of plasma-current was not being accelerated the length of the barrel.

An image converter camera was set up, looking down the barrel of the gun, in order to observe as a function of time the light associated with the plasma blob during its acceleration. This camera was focused on the end of the inner conductor, i.e., in the plane which defined the end of the coaxial region. Rather than a uniform doughnut of light approaching the camera with time, spokes were seen being accelerated. These mottled patches of plasma formed at random and turned (as though the barrel were rifled) as they came out of the muzzle.

Upon reaching the end of the inner electrode at some random point on this electrode's circumference, these pinched spokes stretched and were accelerated into the tank. Probe data showed these tenuous spokes carried only 5000 amp of current, or 2.5% of the main discharge current, as they moved out into the tank. Thus the image converter data confirmed that such a gun operation at low initial input densities (10^{14} particles/cm^3) tends to be unstable.

Plasma Penetration of a Uniform Magnetic Field

In order to examine the penetration of a plasma into a magnetic field, an experiment was set up using the hydromagnetic gun and the vacuum tank into which it fires with one modification. Inside the tank a pair of Helmholtz coils were placed near the end of the gun barrel to generate a B field transverse to the projected axis of the gun. These coils were energized by a 100-μf capacitor operated at 2-kv and switched by an ignitron. The natural period of the system was 60 μsec and the peak field attained was 1 kgauss. By using 20-cm diameter coils and spacing them 10 cm apart, a uniform field was generated in the path of the plasma.

Data were taken with a positive ion detector (LAMS-2570) located 70 cm downstream from the gun. In this way a signal was obtained corresponding to $I = nevA$, where I is the current, n the number of ions, v the velocity, and A the aperture of the detector. By varying the intervening field from zero to 1 kgauss an indication of the field's stopping power was determined from the corresponding variation in detector ion current.

For fields lower than 500 gauss, the single particle detector could not differentiate between the field-on and the field-off cases. The plasma jet penetrated through the field without measurable attenuation. For a field of 1 kgauss, however, the detector could not distinguish a signal above the noise level, which implied a reduction in signal of at least a factor of ten (while the field was changed only by a factor of two). This apparent lack of field penetration for the 1-kgauss field was independently confirmed by photographs taken of the plasma-field interface. Although the pictures were not time-resolved, their interpretation seemed unambiguous, since the duration of the field was long compared with the transit of the plasma. This suggested 750 gauss might be in an interesting transition region.

The 750-gauss barrier was found to cause a delay -- but no reduction in amplitude -- of the detector signal, with the delay averaging 2.5 μsec. Hence, an interpretation in terms of a drift phenomenon was considered. Plasma

densities were a factor of 100 greater than necessary to set up sufficient electric field for an E x B polarization; nevertheless, no detector signals were discernible in the 1-kgauss regime. These data do not however preclude such a penetration because no search was made for blobs deflected off the gun's axis. Also it is possible that the plasma component registered as an ion current does not have sufficient luminosity to be photographed. It is clear such a plasma-field interaction is complicated and more experimental data will be needed before it is understood.

Plasma Penetration of a Line Magnetic Field

To generate a line field, a single straight wire is located 30 cm from the end of the gun and oriented perpendicular to it. This wire is energized by a single 15-μf capacitor; the system is capable of generating a field of 5 kgauss at a radius of 2 cm from the wire. By viewing along the wire with an image converter camera it should be possible to see a plasma-free region surrounding the wire when it is protected by its own fence field. In principle, if the impinging plasma is a good conductor, a parabolic plasma-field interface should be formed while the plasma streams into the field barrier (calculations by Hurley, NYU).

Preliminary results with an argon plasma do show a marked difference in luminosity as a function of fence field, but no clear interface. This is plausible, since an energetic argon ion of velocity 5×10^6 cm/sec in a field of 3 kgauss has a radius of curvature of 0.3 in., i.e., roughly the diameter of the wire. To continue this experiment, therefore, higher fence fields will be required.

G. SCYLLA III

Two methods have been used to determine the electron temperatures (T_e) of the Scylla III plasma in various coil geometries and magnetic compression fields. The soft x-ray spectrometer reported in previous Quarterly Reports (cf. LAMS 2464, p. 17), has been used to observe the continuum radiation in the 5A to 15A region where the intensity is a very sensitive function ($e^{-h\nu/kT_e}$) of the electron temperature. The resolution of the spectrometer makes possible the measurement of the continuum radiation at wavelengths which are free of impurity line radiation. In addition, the spectrometer provides a means of determining the higher Z impurities which are present in the discharge.

The second method of measuring T_e, which was used simultaneously with the spectrometer, utilized a two-absorber soft x-ray detector (LAMS 2464, p. 14). This method provided a time distribution of the soft x-ray emission and T_e. Any impurity line radiations which are present in the transmission regions of the absorber foils will produce an error in the T_e determination by the two-absorber method. The choice of relatively thick absorbers minimized the effects of line radiation. In fact, T_e determined by the spectrometer agreed fairly well with the temperatures determined from the two-absorber detector, showing that the wavelength regions transmitted by the absorbers were relatively free of impurity line radiations.

The results of these measurements are given in Table I. The intensity of continuum radiation increases rapidly with coil length, although T_e remains approximately constant. The increase is much larger than can be explained by simple scaling of plasma volume and magnetic field strength and is not yet understood.

Most of the impurity spectral lines observed in Scylla I are also observed in Scylla III, although the intensities of the lines relative to the continuum are somewhat less than in Scylla I.

Analysis of the two-absorber signals as a function of time and magnetic compression field show the following: (1) The electron temperature

TABLE I

Electron Temperature Data

Coil Length (cm)	Energy Storage (kjoule)	Magnetic Field at Max. T_e (kgauss)	Absorbers	Max. T_e Two-Absorbers (ev)	T_e Spectrometer (ev)	Average T_e (ev)	Stability	Relative Intensity of Soft x-ray Emission
10.6	93	88	Be-Be + Al	580 ± 110	444 ± 50	580 ± 110	Unstable	0.7
18.7	31	44	Be-Be	335 ± 40		335 ± 40	Stable	
18.7	93	94	Be-Be + Al	515 ± 70	475 ± 50	475 ± 50	Stable	22
18.7	94	94	Be-Be	440 ± 60			Stable	
18.7	180	102	Be-Be	340 ± 35		340 ± 35	Unstable	
26.8	93	73	Be-Be	400 ± 35		400 ± 35	Stable	
26.8	180	103	Be-Be	430 ± 50	325 ± 35	380 ± 40	Stable	300

suddenly appears at an appreciable value which is not too different from its peak value at a time when the magnetic compression field is approaching its maximum, i.e., the experimental data do not show a sinusoidal rise of T_e as anticipated in a simple adiabatic compression. A possible explanation of the observed time distribution of T_e on the compression is that free-bound radiations from highly-ionized impurities such as O VIII and O IX dominate the continuum as in Scylla I and that some time is required to produce these highly ionized species. (2) In the cases where the plasma is moderately stable throughout the half cycle, the T_e follows approximately a sinusoidal decompression as the magnetic field decreases. This indicates that the plasma is being contained in the stable cases. (3) When the plasma is violently unstable, T_e undergoes a rapid decrease in the vicinity of the onset time of the instability, as determined previously from streak photographs. The observed decrease in the soft x-ray emission for the unstable cases is more rapid than when neutron emission occurs. These results indicate that the electrons are cooled very rapidly at the onset of the instability, probably as the result of a rapid increase of impurity particles from the wall regions and from a loss of particles.

The various operating conditions used in Scylla III and Scylla I cover a range of maximum magnetic field of 40 to 145 kgauss. Simple adiabatic compression theory provides an approximate correlation between maximum T_e and field strength for $T_e \propto 2B(\gamma-1)/\gamma$, where $\gamma = 5/3$.

As a preliminary to the injection of plasma by guns, Scylla III was operated with a larger compression coil ($l = 30.5$ cm, $d = 11.2$ cm) than previously used. Operation was normal with the production of neutrons and x-rays. The intensity of both x-rays and visible light was less than with the previous smaller coils, indicating a reduction in impurity level in the discharge.

Injected Magnetic Compression Experiment

The two-gun plasma collision apparatus previously reported (LAMS 2570, p. 25) has been adapted to the injection of plasma into Scylla III. Both fast and slow components in the plasma have been trapped and compressed in

the Scylla III field with the production of neutrons. The characteristics of the plasma produced by the collision of the accelerated plasmas in an axial magnetic guide field are that the fastest plasma components (5-10 kev translational energy) have a density of about 10^{14} deuterons/cm^3 and transverse ion energies averaging about 3 kev in the collision region 100 cm from the gun muzzles. At these densities and energies, negligible Coulomb interaction between ions occurs, and the transverse energy is not a result of the plasma intersection. Following the fast component from each gun is a slower plasma, with increasing density and continuous degradation of velocity and transverse energy, which finally attains values of about 10^{16} deuterons/cm^3 and speeds corresponding to ~ 100 ev, but almost no transverse energy. The Coulomb interaction of a beam of ions of this energy and density with a similar beam is so strong as to randomize the directed energy and produce a thermal ion distribution of temperature corresponding to the initial 100 ev translational energy.

The Scylla III coil into which the plasma is injected is 42 cm long with magnetic mirrors at the ends of ratio 1.2. The compression field in the center rises at the rate of 5×10^{10} gauss/sec, reaching a peak value of 70 kgauss in 2.5 μsec. A vacuum chamber of 8 cm inside diameter extends through the compression coil and connects to the guns at each end. The Scylla coil was designed specifically for the experiment and is larger than those previously reported. An axial magnetic guide field, normally 7 kgauss, fills the region between the gun muzzles including the compression coil. The compression field should be capable of trapping ions of the fast component which enter the end of the coil just as the field starts to rise and which have transverse energies roughly equal to or greater than the energy in the axial direction.

In principle it is possible to time the fast-rising field to trap either the faster or the slower plasma components. In addition, the sense of the magnetic guide field can be parallel or antiparallel to the compression field. All four of these combinations have been tried, and all four lead to trapped deuterium plasma producing first half-cycle neutron yields in excess of 10^5 per discharge. The results, under the conditions of optimum timing interval between the two guns and the compression field, are summarized in Table II.

TABLE II

Summary of Neutron Production With Two Plasma Guns Injecting Into Scylla III

Plasma	Guide Field	$\bar{Y}_n$	Y_n(max)
Fast	Parallel	1×10^6	3×10^6
Slow	Parallel	7×10^5	1×10^6
Fast	Antiparallel	3×10^7	6×10^7
Slow	Antiparallel	3×10^7	4×10^7

$\bar{Y}_n$ is the average yield for all shots for which Y_n is greater than 0.25 Y_n (max)

Observations have also been made with injection by one gun alone. The muzzle is then 50 cm from the coil center rather than 100 cm in the two gun arrangement. The results are summarized in Table III.

TABLE III

Summary of Neutron Production with One Coaxial Gun Injecting into Scylla III

Plasma	Guide Field	$\bar{Y}_n$	Y_n(max)	T_e (ev)
Fast	Parallel	7×10^6	1×10^7	undetectable
Slow	Parallel	undetectable	-	-
Fast	Antiparallel	2×10^7	4×10^7	350 ± 50
Slow	Antiparallel	2×10^7	4×10^7	340 ± 70

It is clear from these experiments that the reversed magnetic field can yield significant additional heating in the injected Scylla experiment (LAMS 2444, p. 28). However, neutrons are produced even without trapped reverse field. There can be little question that the ion heating is the result of a simple compression of preheated plasma. The compressed density of trapped particles from the fast component has not been measured directly but is estimated to be of the order of 10^{13} deuterons/cm^3. A comparison of this trapping efficiency of order 10^{-2} with theory is not possible unless the distribution of transverse velocities is experimentally measured. The density of trapped slow plasma from the plasma collision appears to be consistent with

the density and randomized energy inferred in the plasma collision experiment. With one gun alone no slow plasma is trapped in the parallel field case. This is expected for ions with nearly all their energy in axial translation.

The values of T_e in Table III for the one-gun injection experiments were measured with a dual soft x-ray detector. With antiparallel fields the intensities are comparable with those from Scylla III in its normal mode of operation. With injected plasma in the antiparallel field case, a portion of the plasma must certainly reach the tube wall as the external magnetic field passes through zero in the initial stage of the fast compression. Wall impurities introduced in this way may contribute substantially to the soft x-ray intensity. On the other hand, there is no reason to believe that the electrons are particularly hot in the fast plasma parallel field case, and this may account for the low x-ray intensity.

Attempts at streak photography in the axial direction were unsuccessful during the first compression, partially at least, because of light directly from the plasma gun.

These experiments are yielding reaction rates comparable to those of normal Scylla III operation, i.e., slightly preionized flowing cold gas, ionized and shock heated by a sheath which originates at the walls of the tube, although the densities here are perhaps several orders of magnitude lower. The new temperatures are as yet unmeasured but the available information suggests values above 20 kev.

Plasma injection should have considerable advantages over the older Scylla method. The compression region is evacuated and wall contamination should be much less. In addition, there is considerably more freedom in choice of density, since this is not tied to a breakdown process. Contamination can arise from the gun electrodes, but experimental measures to minimize this by time of flight and magnetic filtration between the gun and the coil seem possible. Finally, the high-temperature, low-density regime is favorable for stability, according to a new theory, based on the finiteness of the ion gyro-radius compared to the plasma diameter.

H. E x B ACCELERATOR

The E x B acceleration experiment has been successful in increasing the momentum and energy of the plasma which is injected into the crossed fields from a coaxial gun (cf. LAMS 2570, p. 29). In addition to the acceleration in the crossed fields, several new effects were observed at the higher magnetic fields provided by a new coil allowing fields up to 8.3 kgauss.

A simple technique for finding the path of the plasma stream was to utilize a simple time integrated photograph of the discharge. The direction and intensity as seen in a photograph were in qualitative agreement with the results from the thermocouple and the magnetic probe. However, time-resolved Kerr cell photographs showed that visible light is not present until 4 to 6 μsec after the magnetic or electric field probe signals have passed.

With all the above mentioned techniques, the plasma action in the transverse field was observed with the injection gun at two positions: (1) with the muzzle in the magnetic field and (2) with the muzzle about 10 cm outside the field.

1) Muzzle in B field

With the B field above 5 kgauss, the plasma stream would no longer continue its forward motion into the transverse field and the application of a voltage to the electric field plates had no effect on the progress of the plasma stream. Since the metal gun muzzle would short any electric field that might otherwise develop through polarization, it was felt that a more reasonable operation would result with the muzzle outside the field.

2) Muzzle outside field

With the muzzle 10 cm outside the field the following effects were observed:

a) With fields below 4 kgauss the plasma stream would continue to deflect in the direction of an injected negative particle; however, this was less pronounced than the same effect with the muzzle in the field.

b) It was found that a field of 5-6 kgauss was sufficient to stop the forward motion of the injected plasma. When a 6.5-kgauss field was applied, a thermocouple detector located at x = 50 cm gave a reading of ~ 5% of the zero B field reading (coordinate system defined in Fig. 3). Inspection of time integrated photographs showed the following interesting effect: The plasma, instead of penetrating the field in the initial x-direction, apparently bifurcates and moves horizontally striking the walls on each side. A time integrated photograph of this phenomenon is shown in Fig. 4. The photograph was taken from directly below the glass vacuum chamber, and the direction of injected plasma is shown with an arrow. The phenomenon is reminiscent of the flow of a fluid jet when normally incident on a flat barrier, but instead of changing direction and flowing out radially in a 2π geometry, the plasma flows out in two diametrically opposite channels defined by magnetic field lines. Thus a sufficiently strong magnetic field apparently does not stop the plasma flow but deflects it in two directions normal to the initial velocity. At 6.5-kgauss field, the plasma strikes the glass wall in a region 8 cm high and 4 cm wide beginning just inside the field coil. Magnetic probes indicated that the plasma is sufficiently conducting to exclude ~ 1/3 of the vacuum magnetic field as it enters.

c) A pair of plate electrodes 30 cm long, 15 cm wide, and separated by 7 cm were installed with the leading edge at x = 7 cm (24 cm from injector muzzle). The plates were energized with a 1-μf clamshell capacitor. At a magnetic field of 6.5 kgauss, which the plasma will not ordinarily penetrate, the application of plate voltages as low as V_y = 5 kv allowed a portion of the plasma to penetrate. It was found that with B_Z = 6.5 kgauss and V_y = 20 kv, the thermocouple detected

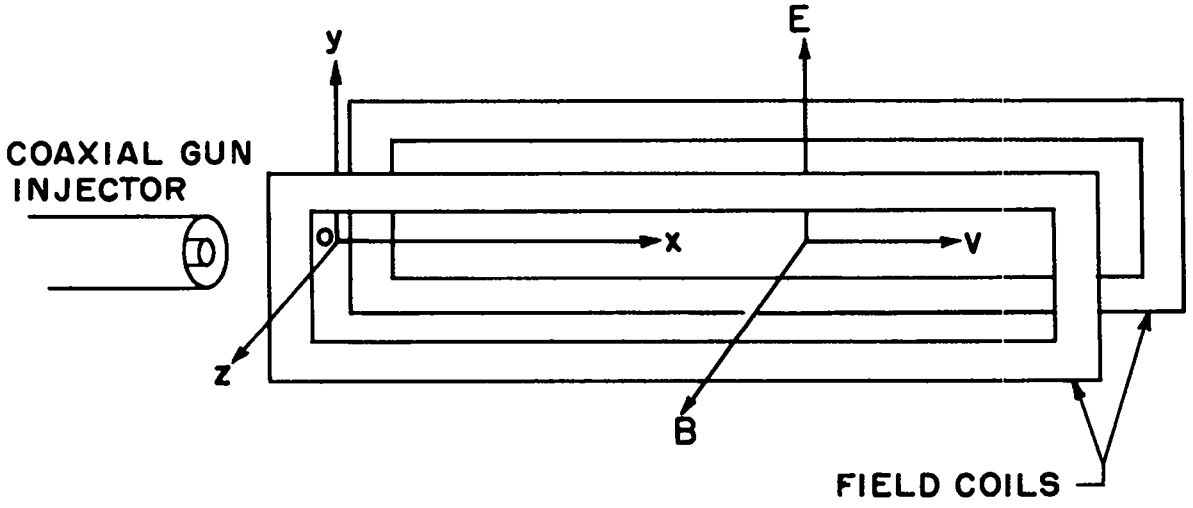

Fig. 3. Coordinate system

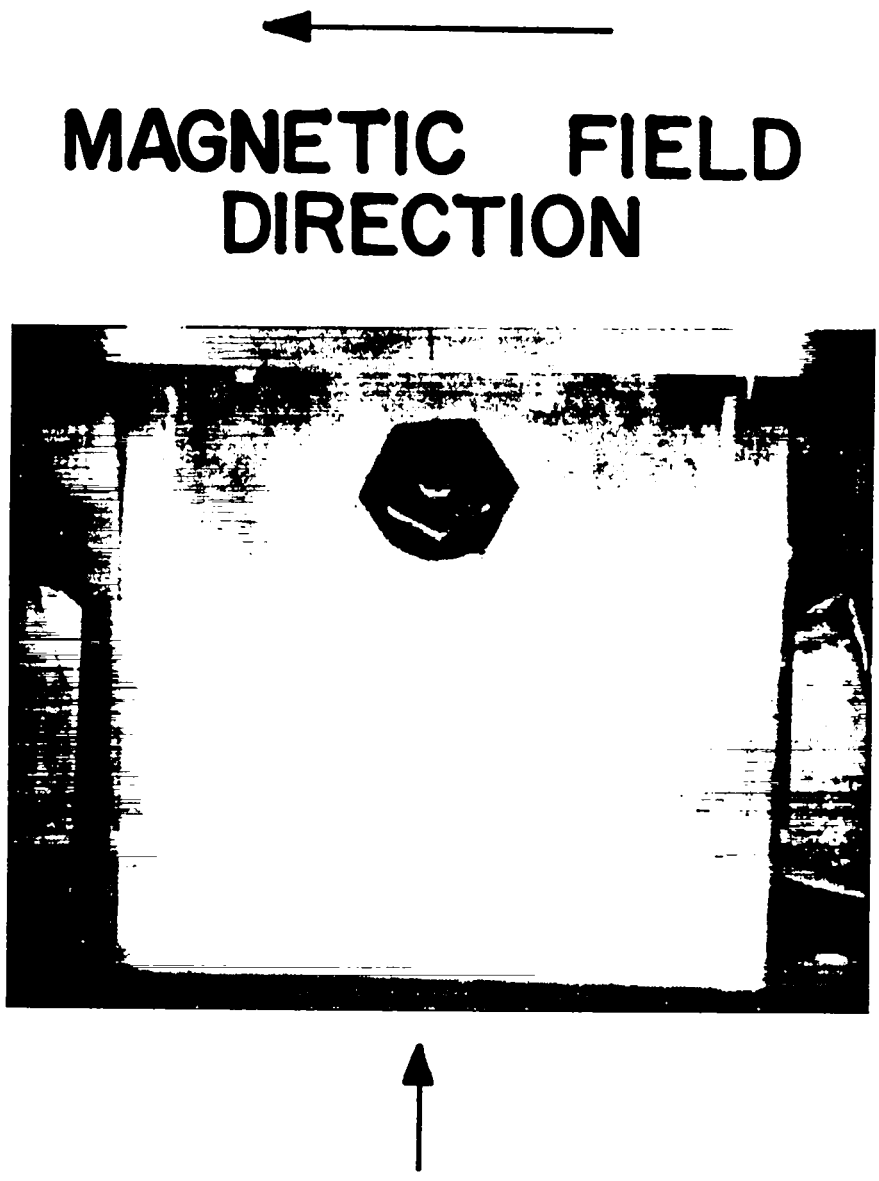

Fig. 4. Time integrated photograph of bifurcated plasma

an increase in transmitted plasma energy of 25% above the 1.6 joules/cm^2 from the injection with $B_Z = 0$ and $V_y = 0$. The transmission property was apparent visually. Photographs of the time integrated light for the case $B_Z = 6.5$ kgauss, $V_y = 0$, and $B_Z = 6.5$ kgauss, $V_y = 20$ kv are shown in Figs. 5 and 6.

d) Since the plasma loads the plate electrode supply rapidly, it was deemed advisable to increase the available energy. The 1-μf clamshell was replaced with a 4.8-μf, 45-mμh Sangamo capacitor. At the same time a nonconducting ballistic pendulum was installed at x = 50 cm to measure the momentum transmitted. It was found that with $B_Z = 6.5$ kgauss, the transmitted momentum increased monotonically with V_y up to 25 kv, the rating of the capacitor. The pendulum indicated that at $B_Z = 6.5$ kgauss and $V_y = 25$ kv the momentum density transmitted was increased a factor of 3 to 4 above the 3 dyne-sec/cm^2 (at x = 50 cm) of the injector alone, i.e., with B_Z and V_y zero.

The results are indeed encouraging from the standpoint of using the linear E x B device as a plasma accelerator.

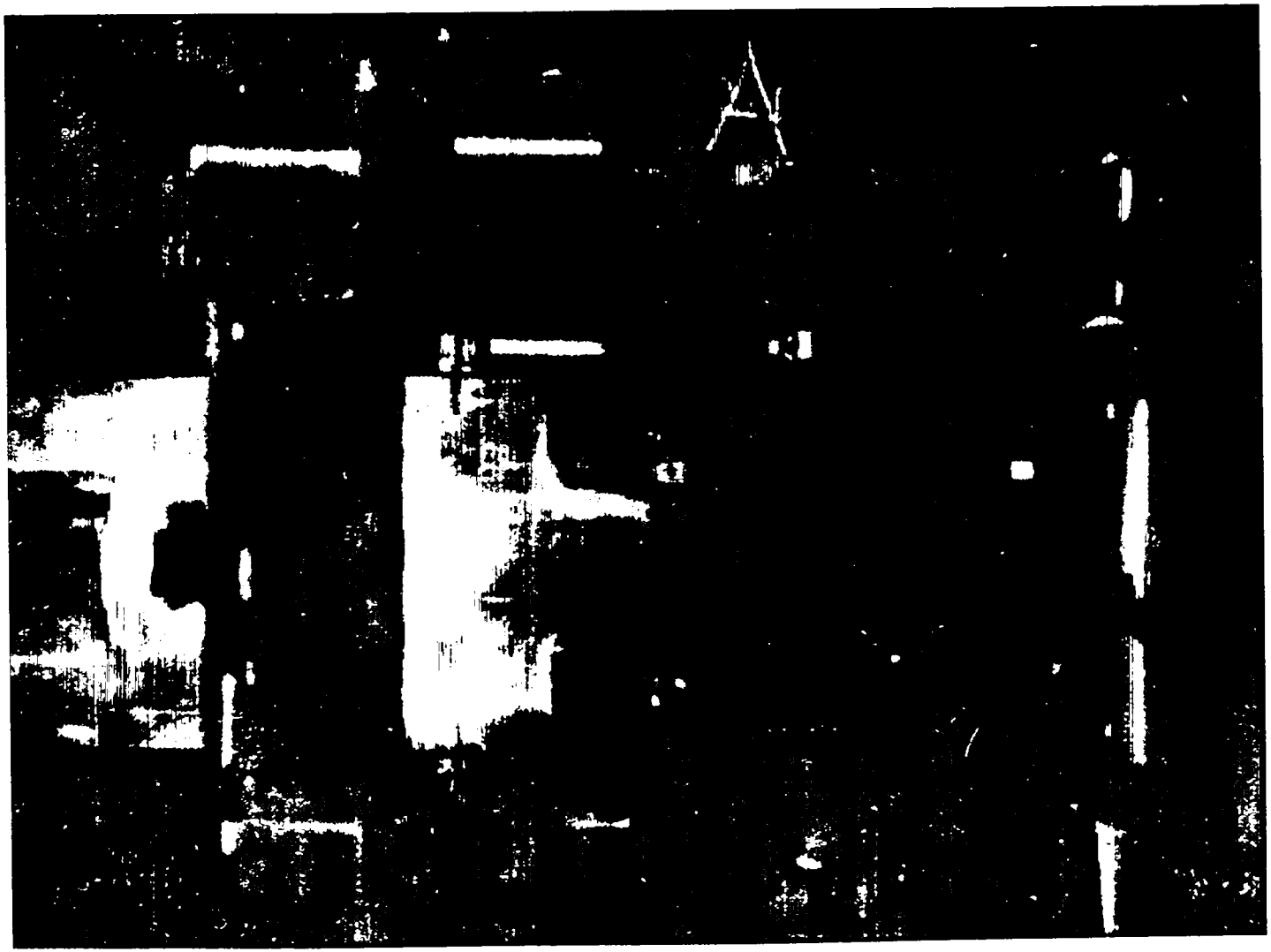

Fig. 5. Time-integrated light for B_z = 6.5 kgauss, V_y = 0

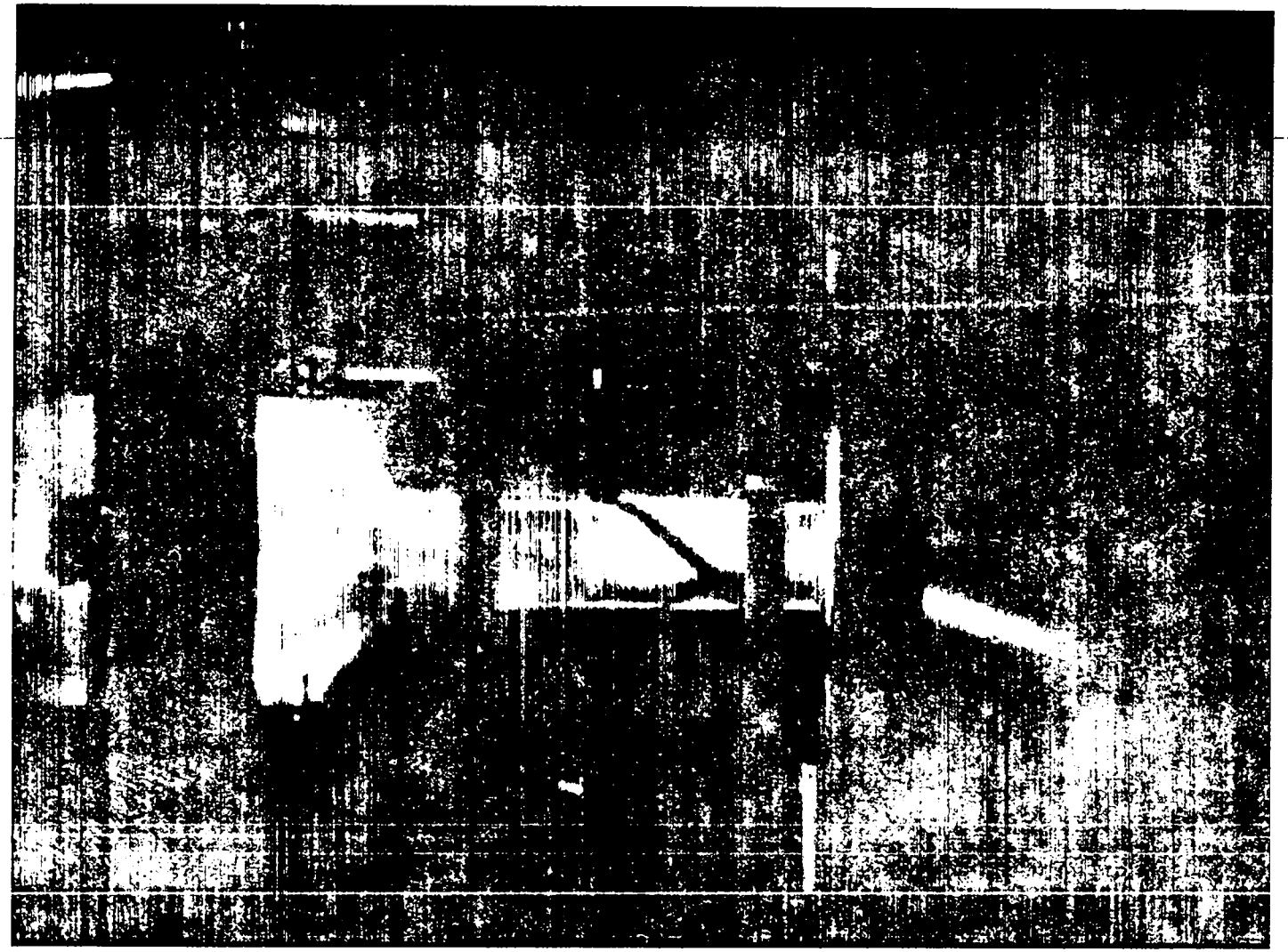

Fig. 6. Time-integrated light for B_z = 6.5 kgauss, V_y = 20 kv

I. SCYLLA I SPECTROSCOPY

In preparation for the Zeeman effect experiment (LAMS 2444, p. 34), it was considered desirable to search the visible spectrum emitted by Scylla I for untabulated lines of Ne IX. There would be a considerable experimental advantage in working with lines at longer wavelengths, which would also have a larger ratio of magnetic splitting to thermal broadening. The Zeeman effect experiment requires the use of spectral lines from highly excited atoms, such as Ne IX, to ensure that the emission is from the hot fireball region of the discharge. A search for the lines on Scylla I made with a photoelectric spectrometer was unsuccessful, probably because of insufficient detector sensitivity.

The lines originally contemplated for the Zeeman experiment, C V and N VI, $1s2s\,^3S_1$ - $1s2p\,^3P_2$ at 2771 A and 1898 A respectively, were found with good intensity and well resolved from the remaining lines of the triplet. The apparatus for the Zeeman effect experiment is now under construction.

J. SCYLLA IV

Progress has been made in the design of the Scylla IV, 3.5-Mjoule magnetic compression experiment. Tables IV and V summarize the design data for the four main capacitor banks. A schematic of the electrical circuit of the banks is shown in Fig. 7.

A report (LAMS 2609) has been prepared covering the extrapolation of the Scylla magnetic compression experiments to higher energies. This report also describes the considerations which have established the parameters of the Scylla IV system.

The status of design work for the main sections of the experiment is given below:

Primary Bank

Test and evaluation of the 50-kv, 2-μf capacitors for the bank has proceeded. A redesign of the high-voltage insulator was necessary and details have been worked out with a manufacturer. The new 50-kv spark gap was tested with the capacitor, and a ringing discharge measurement gave a total inductance for the gap and capacitor of 62 mμh. Further testing, however, showed that the voltage insulation in the cable header was somewhat marginal and that a redesign of this section was necessary. It was finally decided to adopt a design (Fig. 8) in which the gap will be operated under oil. This has two attractive features: (1) The voltage hold off will be conservative and (2) the inductance of the system should be reduced 10 to 20%.

The layout of the bank is shown in Figs. 9 and 10. The design for the 50-kv racks has been completed and will be sent out for fabrication as soon as tests are completed on the 50-kv capacitor. The capacitor platform is in the final stages of design.

Preionization Bank

The design of the preionization bank has received considerable attention. Since its inductance may be very critical to one phase of the

TABLE IV

Scylla IV System Parameters

Parameter	Unit	Primary Bank	Secondary Bank (Zeus)	P.I. Bank	B_o Bank
V	kv	50	20	60	10
C	μf	432	15,000	17	5600
W	kjoule	540	2940	30.6	280
*L_{bank}	mμh	0.29	1.3	5	40
L_{cables}	mμh	0.48	1.13	3.25	1000
$L_{hdr + coll. plate}$	mμh	1.40	3.00	0.86	15.50
L_{source}	mμh	2.17	5.46	9.1	1055
L_{total}	mμh	12.2	15.5	19.1	1065
$\lambda = \frac{L_{source}}{L_{coil}}$		0.22	0.55	0.91	106
**Energy Transfer	%	82.2	64.7	52.3	0.9
$\tau/4$	μsec	3.6	23.9	0.9	121
I_{max}	Mamp	9.4	19.7	1.8	0.7
B_{max}	kgauss	118	246	22	9.1

* Bank - capacitors, switches and switch header

** $1/(1 + \lambda)$

TABLE V

Scylla IV Component Parameters

Parameter	Unit	Primary Bank	Secondary Bank	P.I. Bank	B_o Bank
No. of Cap.		216	1008	20	96
C/cap	μf	2	14.8	0.85	58.3
W/cap	kjoules	2.5	2.9	1.5	3
L/cap	mμh	16	40	40	60
Type of sw.		Spark gap	Ignitron	Spark gap	Ignitron
No. of sw.		216	336	20	32
Cable type		17/14	17/14	19/14	RG 17/U
Cable length	ft	17	21	13	400
No. of cables/sw.		6	2	10	1
No. of cables		1296	672	100	32
L/ft of cable	mμh	36	36	50	86
L/cable	mμh	612	755	600	8600
L_{header}	mμh	0.15	0.50	0.13	13.0
$L_{collector\ plates}$	mμh	1.25	2.50	0.74	2.50

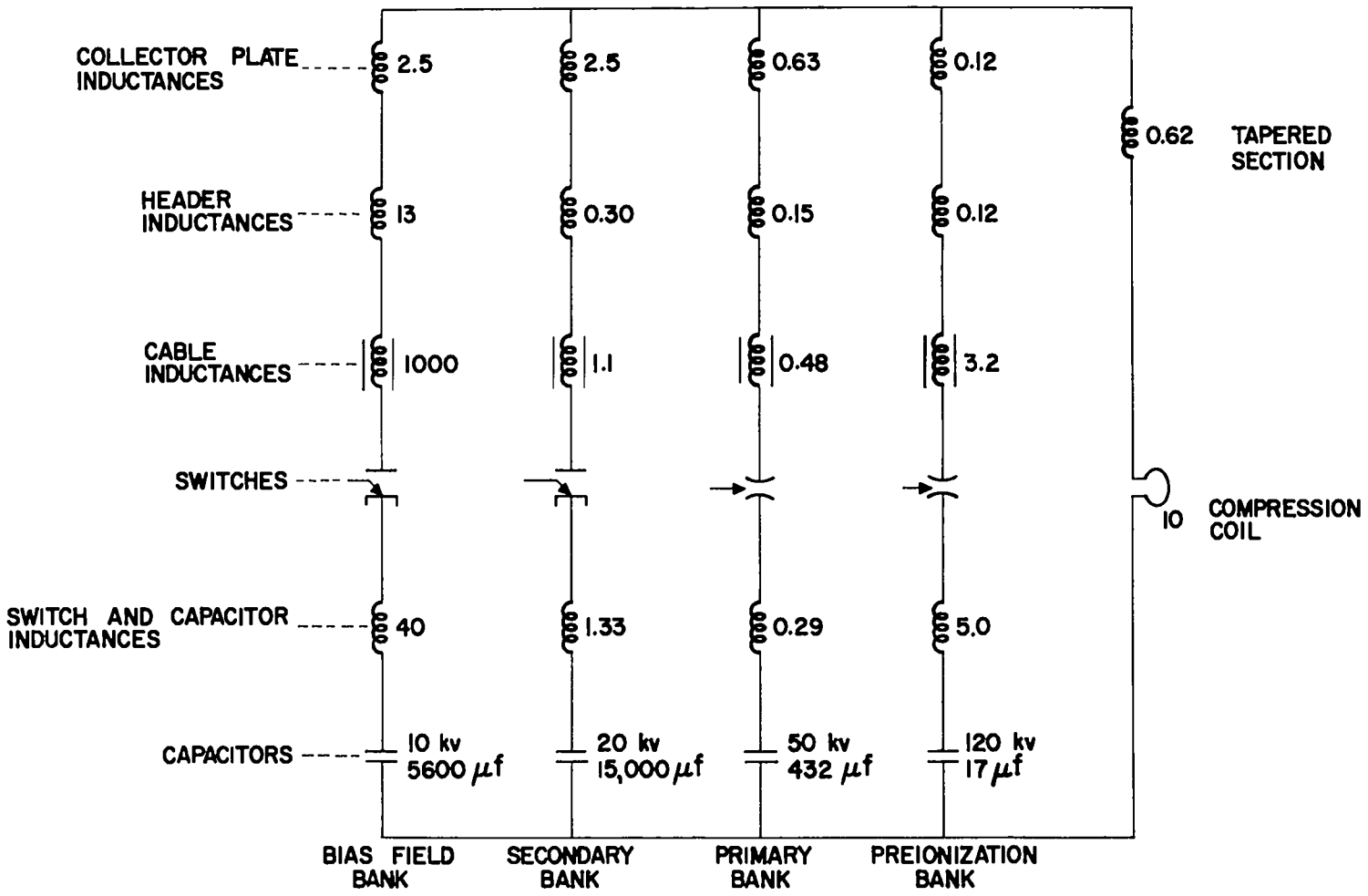

Fig. 7. Schematic circuit diagram of the Scylla IV energy storage system. Inductances are given in mμh.

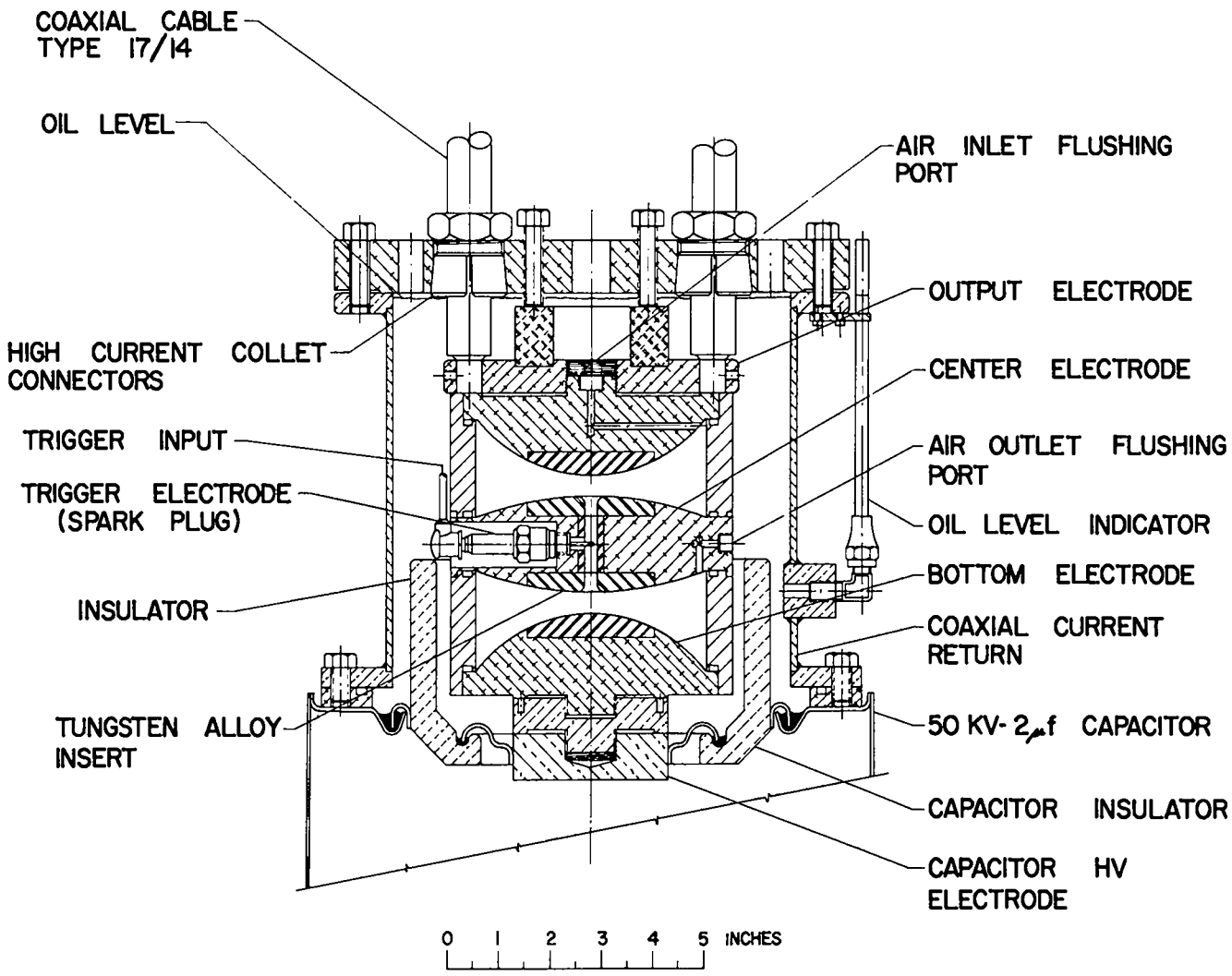

Fig. 8. The 50-kv spark gap and capacitor header to be used in the primary capacitor bank.

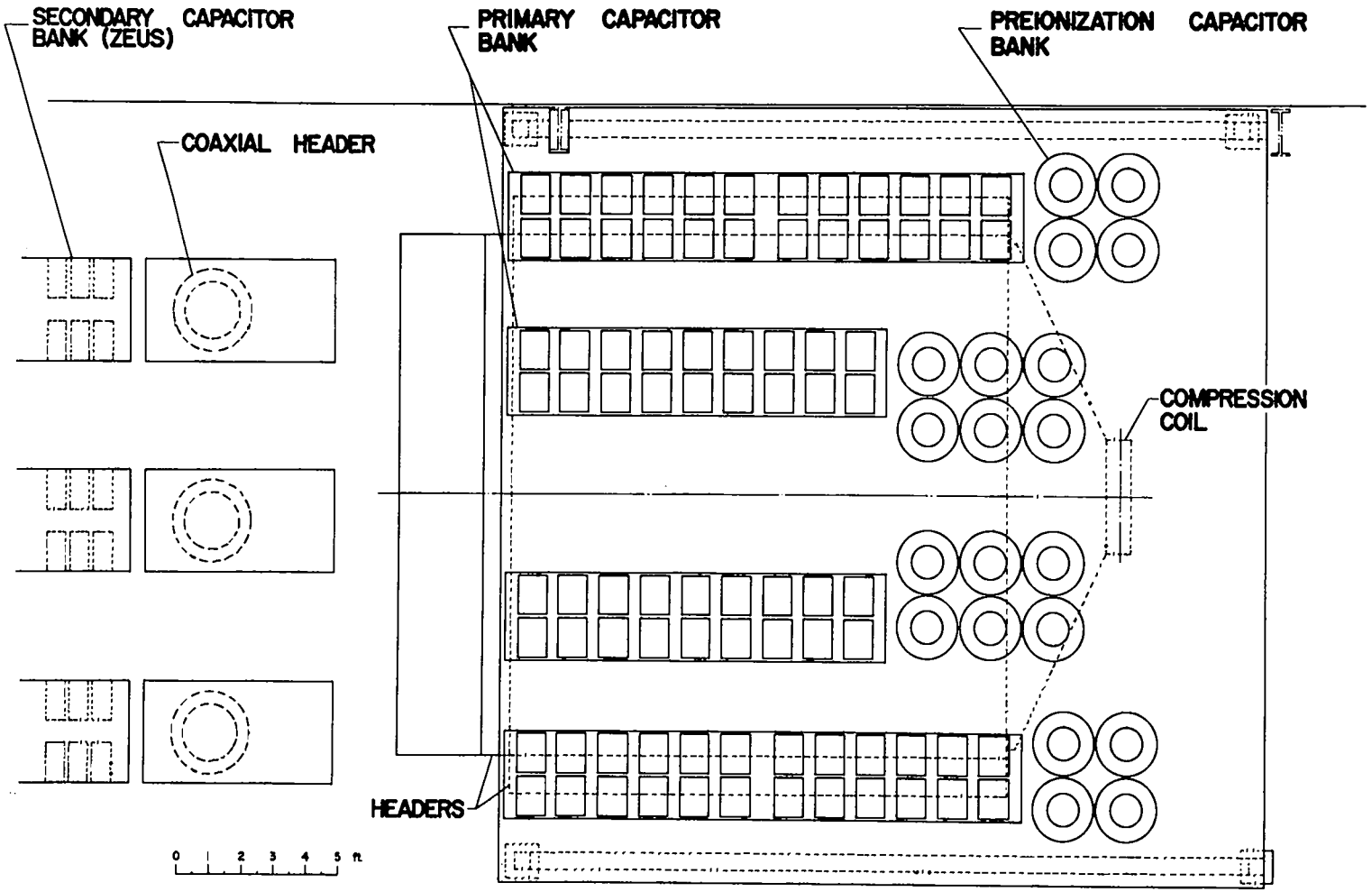

Fig. 9. Plan of the Scylla IV capacitor banks with the position of the collector plates and headers shown by the dashed lines.

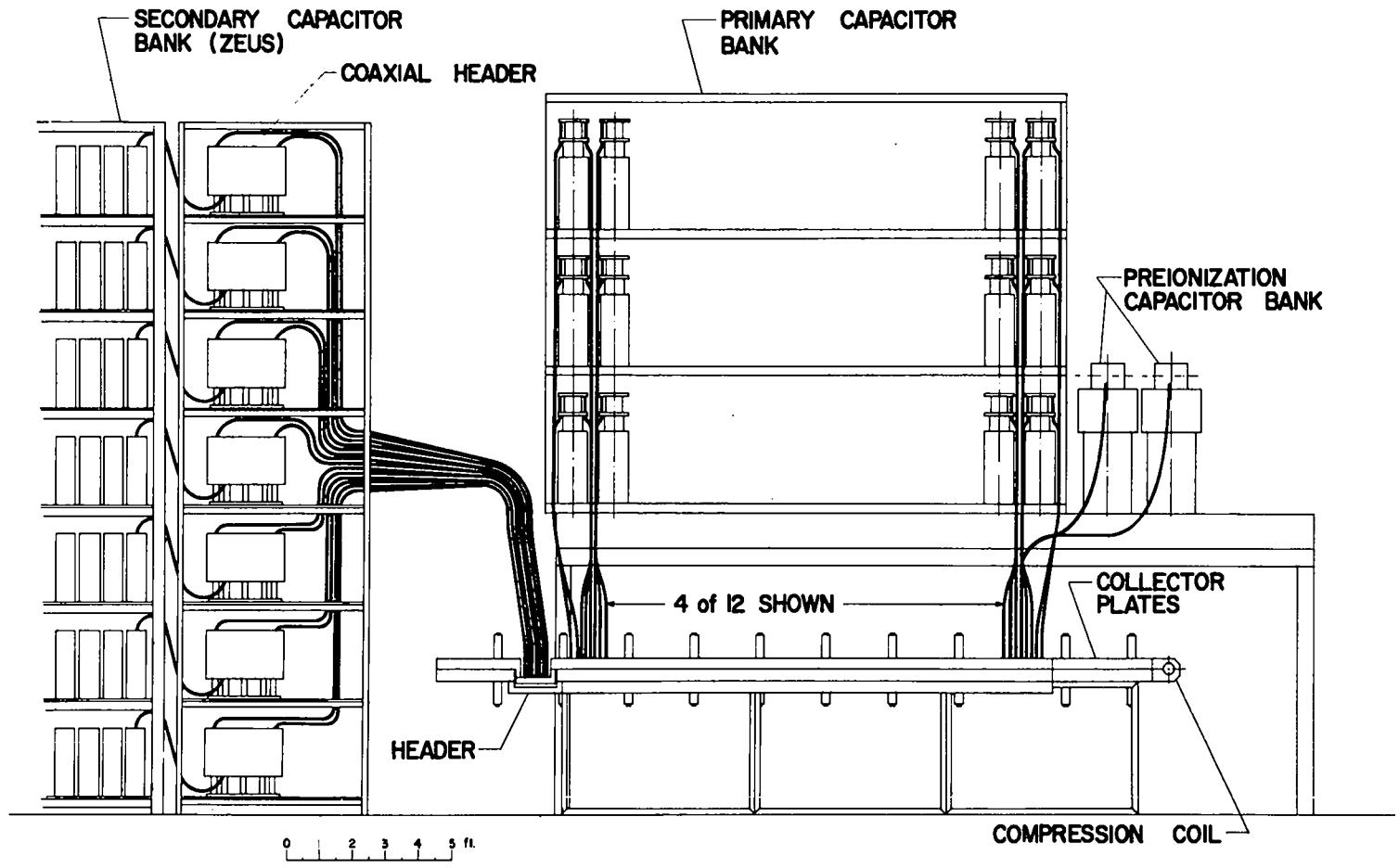

Fig. 10. Side elevation of the Scylla IV system.

experiment, every attempt has been made to reduce it to the lowest possible value. The arrangement of the bank capacitors has been adjusted to give the minimum cable length consistent with the isolation that is required for reliable firing of the 20 spark gaps in parallel. The design of the spark gap has been such as to minimize its inductance in this application. The design of the capacitor has been reviewed with two manufacturers and two different units have been ordered for test and evaluation. It appears possible to reduce the inductance of the 0.85-μf, 120-kv capacitor from approximately 90 to 30 mμh.

Secondary Bank

Testing has continued on the fast shelf design reported previously. A special rack for holding the low-inductance transmission system cables was installed on one shelf of Zeus. The coaxial switch header was re-installed after some modifications and the new lumped-inductance coils were connected in series with each cable between the capacitors and the header. The use of these coils will reduce the total cable required on each shelf by a factor of about two. Failure of some of these coils when a capacitor shorts has required a revision of the design. However, under normal operation the coils have performed satisfactorily, showing that the system is practical in principle.

The cable collector system for the 404 cables connecting Zeus to the header-transmission system has been designed.

Header and Collector Plates

The basic design for the cable header and collector plate system has been developed. The system is shown in Fig. 11. The collector plates are 15 ft on a side and will have 0.060 in. of Durathene insulation between them. The plates will be made of 2 in. aluminum with reinforcing webbing. They will be held together with an extensive system of insulated through bolts.

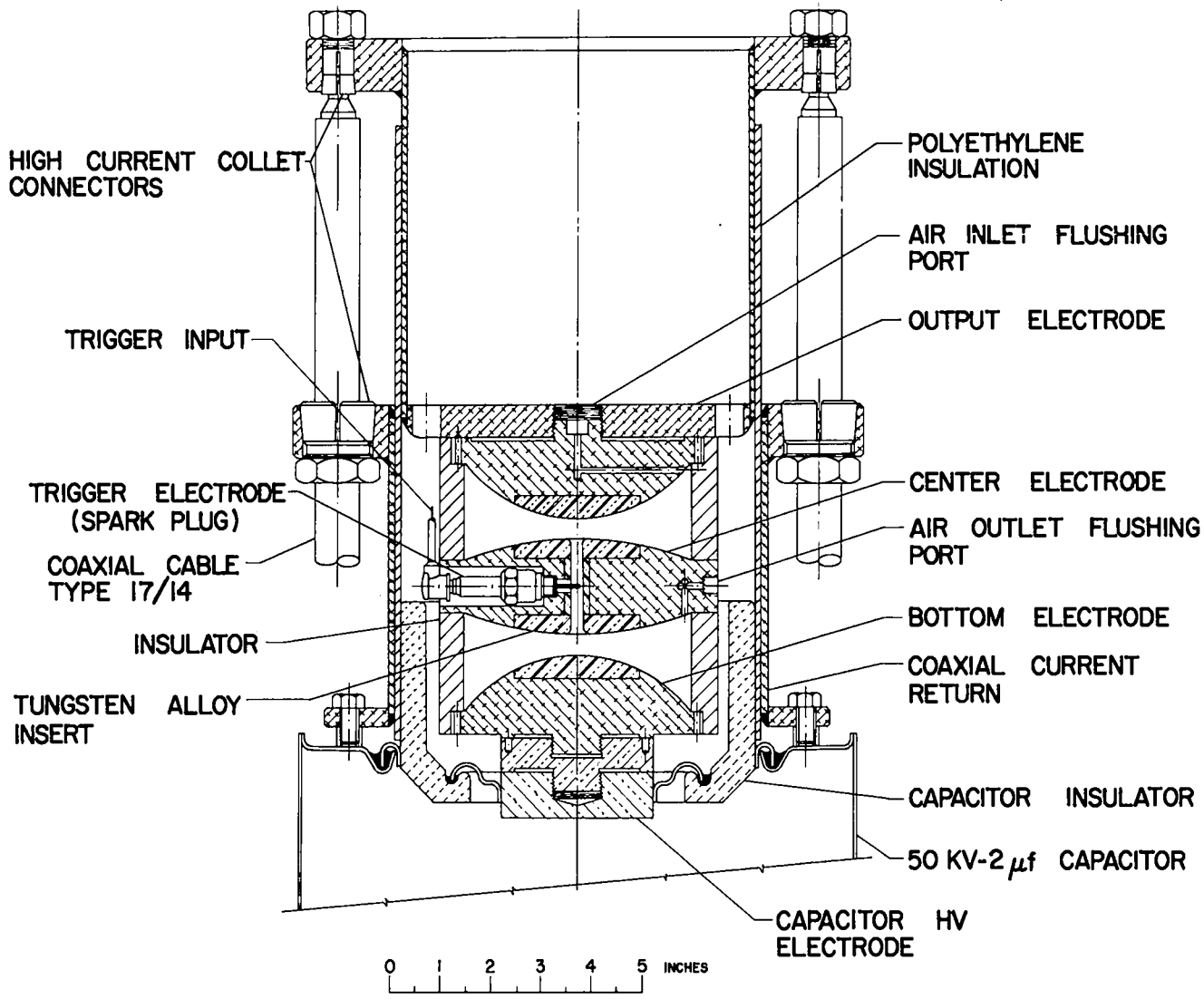

Fig. 11. Collector plates and header arrangement of Scylla IV with a detailed section of the header.

Installation

Work has proceeded on the plans for the installation of the Scylla IV system adjacent to the Zeus capacitor bank. The philosophy of control of the experiment has been developed and work is proceeding towards incorporating the system into the Zeus control system. Plans are also proceeding for the installation of the required utilities and associated equipment for the experiment.